

Supporting information

Thermally Expanded Graphite: A promising anode electrode in the current and next-generation LIBs

Sarmin Hamidi^{a,b}, Kasra Askari^{a,b}, Pejman Salimi^{ b, c}*

^a Electrochemical Energy Systems Research Office, Sharif Technology Services Complex, Sharif University of Technology, Tehran, Iran

^b Eshtad Energy Engineering Co., Guilan Science and Technology Park, Rasht, Iran

^c Istituto Italiano di Tecnologia, Via Morego 30, 16163 Genova, Italy

1- Experimental

1-1- Materials and method

To exfoliate and expand graphite, first of all, modified advanced natural graphite battery-grade powder called ANG (Sigma-Aldrich) which is also known as flake graphite was put in the electrical oven at 45°C for 6h. Then the graphite, KMNO₄ and HNO₃ 65% (Merck) were mixed by a glass rod in Pyrex glass jar at room temperature for 6h. The weight ratio of raw graphite, KMNO₄, and HNO₃ were 1:1:2. According to literature¹ the maximum expansion ratio (expansion ratio defined as the ratio of expanded graphite volume per original graphite mass (e.g. ml/g)) could be achieved in the mentioned mixing ratio. In the next step, the mixture was placed into a microwave oven and irradiated at power of 900 W and 2.5 GHz for 150 seconds. The obtained worm-shaped TEG was dispersed in benzyl alcohol (Sigma Aldrich) and was stirred for 24 hours at 80 °C. The mixture was poured into ethanol (459828 Sigma-Aldrich) solution and pulverized by the ultrasonic cell crusher (SCIENTZ) for 30 min and dried in a vacuum oven at 60°C for 24 h to obtain the TEG powder.

1-2- Structural Characterization

X-Ray Diffraction (XRD) was carried by Philips X'pert MPD diffractometer equipped with a 1.8 kW CuK α sealed ceramic tube. Raman spectroscopy analysis was done by HORIBA XploRA Plus

(Japan) instrument with 532 nm (Edge) laser Raman spectrometer, 750 nm grating, and 100 μm slit. XRD and Raman was performed to determine the crystallinity, the interlayer spacing, and order/disorder degree of the structure of the samples. Fourier transform infrared spectra (FT-IR) were recorded by BRUKER platinum ATR spectrometer to identify the functional groups in the samples. Scanning Electron Microscopy (SEM) was carried out to observe the morphology of materials. SEM was performed by FE-SEM ZEISS SIGMA VP (Germany) in different magnification. The weight percent of elements that existed in both TEG and raw graphite was determined with Energy Dispersive X-Ray Spectroscopy (EDS), mapping and line scanning analysis by FE-SEM ZEISS SIGMAVP Oxford Instrument detector. Surface analysis was carried out by Brunauer–Emmett–Teller (BET) Quantachrome NOVA4200e (USA) device at 150 °C degassing for 5 hours under 100 mTorr vacuum.

1-3- Electrode preparation, Cell assembly, and Electrochemical measurements

For preparing electrodes, polyvinylidene fluoride (PVdF) binder was dissolved in N-methyl-2-pyrrolidone (NMP) solvent. Then, active material (TEG or ANG) and carbon black were added to the PVdF solution. The weight ratio of active material (TEG and ANG), carbon black, and PVDF were 80, 10, and 10 wt%, respectively. Afterward, the slurry was ground with mortar until reaching complete homogeneity and, through doctor blade technique, a 300 μm layer was cast on a copper foil, which was then dried for 8h in a vacuum oven at 100 °C. The dried electrode film was punched into disks, providing $\sim 7.5 \text{ mg cm}^{-2}$ of active material mass loading. After introducing the electrode into the glove box (MBraun with oxygen and water contents below 0.1 ppm) the 2032-coin cells were assembled using the working electrodes, Li metal chips (Gelion, battery grade) as the counter and reference electrodes, and micropores Celgard 3501 membrane as the separator. The LP30 electrolyte (1 M LiPF_6 in a 1:1 (v/v) solution of ethylene carbonate/dimethyl carbonate-Merck, battery grade), and ether-based electrolyte (1.0 mol kg^{-1} of bis(trifluoromethane) sulfonimide lithium salt (LiTFSI) with the addition of 0.5 mol kg^{-1} of lithium nitrate (LiNO_3) in the mixture 1:1 w/w of 1,3-dioxolane (DOL) and 1,2-dimethoxyethane (DME)) were used for conventional and next-generation batteries, respectively. The procedure for ether-based electrolyte preparation is reported elsewhere^{2,3}.

The cycling and rate performance analyses of the half-cells were carried out in the voltage range of 0.01–2.5 V. Electrochemical impedance spectroscopy (EIS) were performed in a frequency range between 100 kHz to 10 mHz under open circuit conditions with 10 mV of alternating current and the obtained data were fitted with Z-view software.

For the full cell analysis, the TEG anode was prelithiated in the presence of LP30 electrolyte using the lithium direct contact electrochemical method². The procedure for anode prelithiation and capacity balancing of cathode and anode is reported in our previous work⁴. Commercial LiFePO₄ (LFP-NEI corporation) was used as cathode to couple with the prelithiated TEG. The mass loading of a single- coated LFP cathode on aluminum foil was 14.5 mg cm⁻². The same electrolyte (LP30) and separator used in the half cell were applied in the full cell. In the voltage window of 1.25-3.9 V, the assembled full cell was charged and discharged.

All the tests were run at room temperature after 12h rest. The instrument PGSTAT30 (Metrohm, USA) was used for electrochemical analyses.

2- Characterization results and discussion

Figure S1 shows the elemental distribution on the surface of TEG and ANG by EDS spectrum. The content of Fe element in TEG is more than that of ANG. The high theoretical specific of Fe could be helpful to improve the capacity of the electrode materials in LIBs⁵. Additionally, the amount of C and N has been decreased through thermal exfoliation. This could be related to the evaporation of some elements such as Carbon (CO₂) and Nitrogen (NO₂) through microwave irradiation^{6,7,8}. The line scanning and EDS mapping of TEG sample are also provided in Figure S1 to show the changes of wt% of elements diversity in a line of sample and whole of TEG surface in 25 μm.

The XRD pattern of TEG (Figure 1c, main manuscript) exhibits a sharp peak at around 26° which is associated with the (002) plane⁹. Additionally, the other weak peak at around 55° is related to (004) plane of the hexagonal graphitic structure (JCPDS No. 00–008-0415⁹). Can be concluded from the scattered pattern of TEG that the carbon is a graphite-2H material with Hexagonal crystal lattice and p63 space group. According to Braggs law, the interlayer spacing (d-spacing) between two graphene layers is about 3.41 Å, while the regular value of d-spacing for graphite is 3.35 Å (The XRD of ANG is provided in Figure S2a). This is because the insertion of heteroatoms such

as C-O-C, C-OH, and -COO groups at the edges and flaws caused the expansion of graphitic layer¹⁰.

Raman spectra of ANG and TEG are provided in (Figure 1d, main manuscript). According to this analysis, a significant structural change occurred after the chemo-thermal process. The intensity of D bands (1340 cm^{-1} , corresponds to the disordered structure of carbon), G bands (1570 cm^{-1} , refers to the graphitic structure and sp^2 planar structure), and G' (2D, 2700 cm^{-1} , overtone of D bands) for TEG are more than those of ANG sample. In fact, the exfoliation by applying the intercalating agent and thermal shock led to high crystalline graphite with more sp^2 hybridized C-C bonds. Additionally, high intensity of G bands indicates that the carbon of TEG is rich in graphitic phase¹¹. The intensity ratio of D to G bands (i_D/i_G) that reveals the disordered degree of carbon materials, is equal to 0.314 and 0.423 for TEG, and ANG, respectively. This result indicates that thermal shock exfoliation led to increase the size of sp^2 plane, strengthening graphite-ordered structure, reduce disordering degree and edge planes¹¹.

FT-IR (Figure 1e, main manuscript). analysis is useful to determine the functional groups of the samples. The characteristic peaks at $2800\text{-}3000\text{ cm}^{-1}$ are attributed to the C-H Stretching of Alkene¹². The characteristic peaks related to C=O stretching vibration are clear with the range of bands at $1750\text{-}1850\text{ cm}^{-1}$ and $1050\text{-}1200\text{ cm}^{-1}$ which has intensified for TEG. This could be related to the oxidization process by KMnO_4 ¹³. Graphite carbon hexagonal ring leads to characteristic peaks at $1970\text{-}2170$ and $1550\text{-}1650\text{ cm}^{-1}$ region that belongs to C=C=C and C=C stretching vibration, respectively. Furthermore, the sharp characteristic peaks at 650 cm^{-1} and $790\text{-}880\text{ cm}^{-1}$ are related to C=C bending¹². Skeletal vibration of Graphene sheets (GS) appeared at 1580 cm^{-1} . According to the sharper peaks in TEG compared to ANG, it can be claimed that carbon atoms were packed in a hexagonal structure of graphite. Moreover, there are small peaks in the range of $1100\text{-}1400\text{ cm}^{-1}$ which might be associated with C-N and C-O¹².

According to nitrogen adsorption/desorption analysis (Figure S2 b, and c), the BET specific surface area (SSA) of ANG and TEG are equal to 12.8 and $52\text{ m}^2\text{g}^{-1}$, respectively. On the other hand, BJH method cumulative presents pore size distribution and surface-active area of both graphite in the nitrogen adsorption/desorption that for TEG and ANG are equal 71.9 , $78.3\text{ m}^2\text{g}^{-1}$ and 15.6 , $17.3\text{ m}^2\text{g}^{-1}$, respectively. The result of BET and BJH method show the surface area increases by the thermal shock. Also, the total pore volume with diameter less than 396.54 nm at

$P/P_0 = 0.995151$ for TEG is equal to 0.0976 cc/g and for ANG is 0.01592 cc/g . Additionally, the average pore diameter for TEG (7.507 nm) is greater than the pore diameters for ANG (4.959 nm).

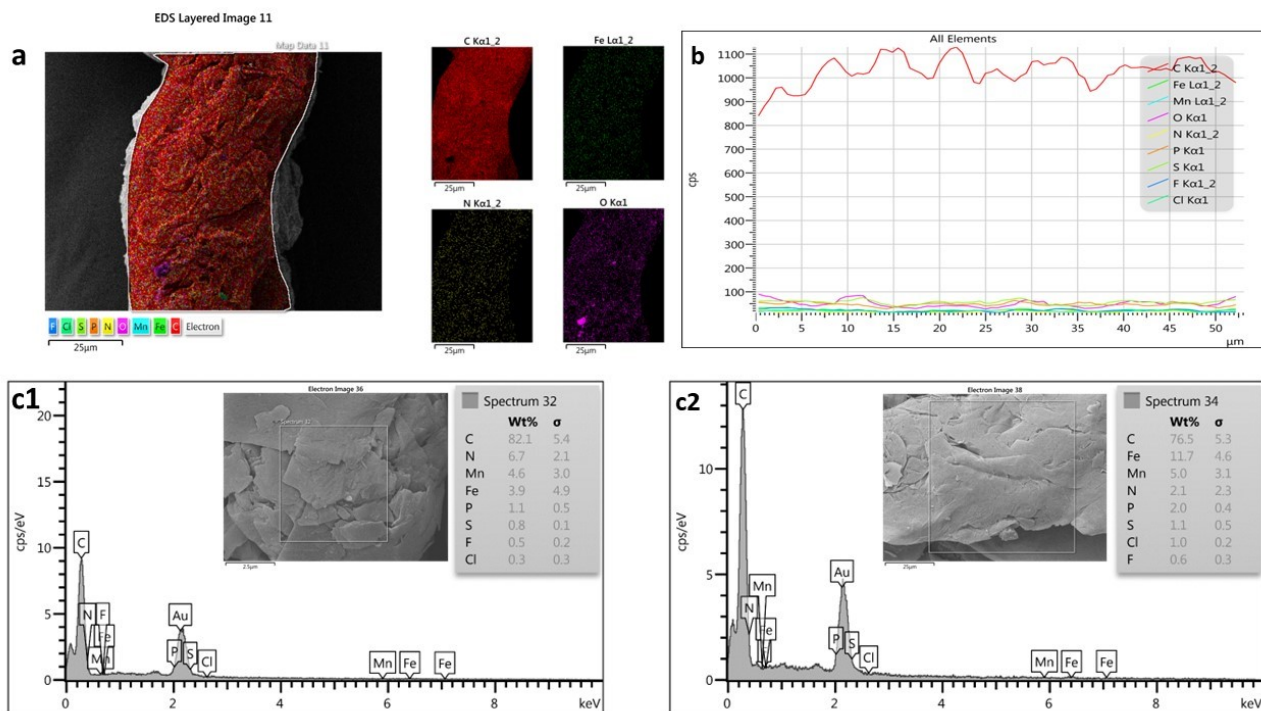


Figure S1. Mapping analysis of TEG (a), Line Scanning analysis of TEG (b), Energy-Dispersive X-ray Spectroscopy analysis of ANG (c1), TEG (c2).

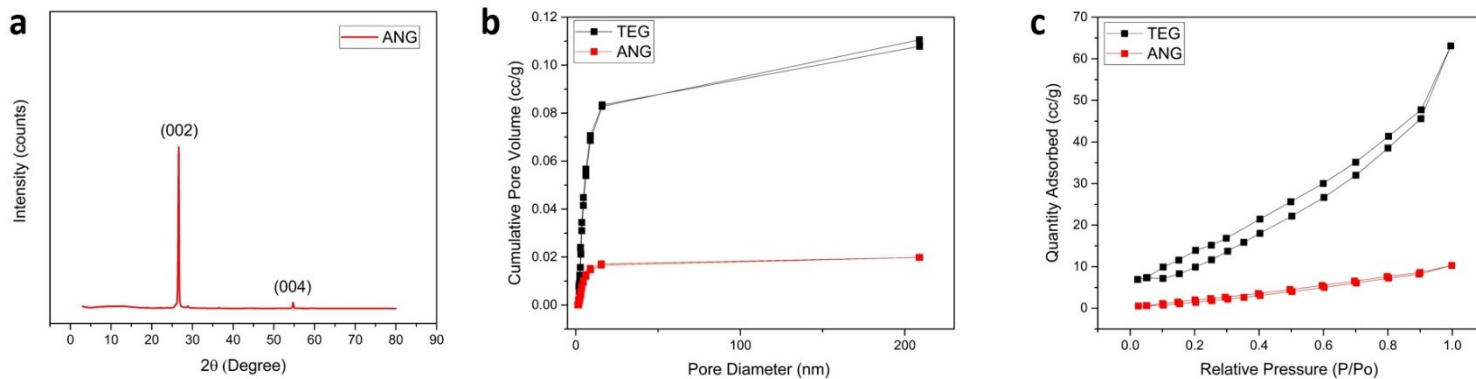


Figure S2. XRD pattern of ANG (a), BJH pore size distribution adsorption/desorption (b), and Isotherm linear adsorption/desorption of TEG (black line) and ANG (red line) (c).

References

1. Kim, J. et al. Scientific Cooperations International Workshops on Engineering Branches **1**, 273–277 (2014).
2. Salimi, P. et al. Energy and Environmental Materials 1–9 (2022) doi:10.1002/eem2.12567.
3. Venezia, E., Salimi, P., Chauque, S. & Proietti Zaccaria, R. Nanomaterials **12**, 3933 (2022).
4. Parviz, Z. et al. ACS Appl Energy Mater **5**, 15155–15165 (2022).
5. Zheng, F. et al. J Alloys Compd **693**, 1197–1204 (2017).
6. Yakovlev, A. V., Finaenov, A. I., Zabud'kov, S. L. & Yakovleva, E. V. Russian Journal of Applied Chemistry **79**, 1741–1751 (2006).
7. Forsman, W. C., Vogel, F. L., Carl, D. E. & Hoffman, J. Carbon N Y **16**, 269–271 (1978).
8. Wei, T., Fan, Z., Luo, G., Zheng, C. & Xie, D. Carbon N Y **47**, 337–339 (2009).
9. Chen, Z. et al. Mater Lett **229**, 134–137 (2018).
10. Wen, Y. et al. Nat Commun **5**, 1–10 (2014).
11. Qian, W., Sun, F., Xu, Y., Qiu, L., Liu, C., Wang, S., & Yan, F. Energy Environ. Sci., 7(1), 379–386 (2014)
11. Yang, S., Li, L., Xiao, T., Zhang, Y. & Zheng, D. Sep Purif Technol **160**, 81–88 (2016).
12. Peng, T., Liu, B., Gao, X., Luo, L. & Sun, H. Appl Surf Sci **444**, 800–810 (2018).